OPEN ACCESS

Tuning the Products of CO_2 Electroreduction on a Ni_3Ga Catalyst Using Carbon Solid Supports

Tuning the Products of CO_2 Electroreduction on a Ni_3Ga Catalyst Using Carbon Solid Supports

Aubrey R. Paris, An T. Chu, Conor B. O'Brien, Jessica J. Frick, Sonja A. Francis,* and Andrew B. Bocarsly *,z

Department of Chemistry, Princeton University, Princeton, New Jersey 08544, USA

Certain alloys of nickel have recently been shown to reduce CO_2 to multi-carbon products electrochemically without the need for copper. Here we show that Ni_3Ga thin film electrocatalysts on carbon electrodes discriminate between CO_2 reduction pathways and products based on their surface morphologies, which are controlled by catalyst-carbon support interactions. It is also observed that unsupported, bulk Ni_3Ga reduces CO but not CO_2. With this understanding, a tandem electrocatalyst utilizing two variants of the Ni_3Ga material—one supported and one unsupported—was developed. In this two-electrode system, CO is generated from CO_2 on an electrode optimized for this process, and the CO is then further reduced to methanol in the same reactor. It appears that choice of carbon support impacts the morphology of Ni_3Ga during the synthesis of the catalyst, thereby influencing the electrolysis product distribution.

 [DOI: 10.1149/2.0791807jes]

Manuscript submitted February 16, 2018; revised manuscript received April 9, 2018. Published May 15, 2018.

The discovery or design of CO_2 reduction catalysts has been a focus of current electrochemical studies due to the rising concentration of CO_2 in the atmosphere coupled with global challenges accompanying such a phenomenon.[1,2] Materials that facilitate the transformation of CO_2 are wide-ranging, but a deficiency in our understanding of how they function is exemplified by several recent studies reporting on what is nominally the same electrode material after modifying the structure, morphology, or composition and eliciting a new or improved response toward CO_2 reduction.[3–10]

When a known CO_2-reducing material is altered to include novel structures or morphologies, it is anticipated that the newly introduced characteristic may change the base material's activity by increasing the concentration of surface active sites or improving intermediate stability, thereby impacting catalysis. As an example, the Kanan group has reported that copper catalyst morphology influences the distribution and faradaic efficiencies of CO_2 reduction products.[11] The importance of morphology is one reason why nanoparticles and thin films have garnered attention. Selection of heterogeneous catalysts in non-bulk form involves immobilizing nanoparticles, thin films, and other specialty structures on electrodes, and thus a second material, the solid support, is added to the electrochemical system.

It is well-established that solid support identity can directly impact material or catalytic properties. For example, Rakhi et al. grew Co_3O_4 nanowires on carbon fiber paper and planar graphitized carbon paper and achieved startlingly different morphologies,[12] while other authors witnessed similar morphological impacts for different systems.[13,14] Superconductivity,[15,16] material hardness,[17] and especially catalytic efficacy in the oxygen reduction reaction[18–21] have been attributed to solid supports interacting with or changing properties of surface materials that are typically the focus of the study. These works suggest that properties such as catalyst morphology, which is important for CO_2 electrocatalysis, may be intimately tied to solid support identity.

Many solid supports ranging from Ag metal[7] to Ti-based nanotube arrays[22] have been employed in electrocatalytic CO_2 reduction, but carbon-based supports are by far the most widely used for this purpose, as summarized by Yang and coworkers.[23] These carbon supports vary in terms of their structural and electronic properties and surface functionalities[24] and, importantly, some researchers have noted a carbon solid support dependence in electrochemical CO_2 reduction with copper-based catalysts.[25] Recently, a new class of copper-free, carbon-supported, nickel alloy catalysts for CO_2 electroreduction to multi-carbon, multi-electron products has been described. These catalysts include the Ni-Ga electroreduction system analyzed by Torelli et al.[26] and Ni_3Al electrocatalyst reported by our lab.[27] Efficacy of the Ni-Ga system, in particular, has been examined with respect to alloy composition,[26] but solid support and morphological impacts on its behavior toward CO_2 have yet to be discussed. We report here that these factors are important in maximizing the system's ability to generate its highly interesting CO_2 reduction products, which are currently limited to faradaic efficiencies below 2%.[26]

Herein, the electrochemical activity of five different Ni_3Ga morphologies are compared: thin films on (1) highly ordered pyrolytic graphite (HOPG), (2) glassy carbon, and (3) reticulated vitreous carbon (RVC) solid supports; (4) Ni_3Ga nanoparticles; and (5) unsupported, bulk alloy. For this study, we focused on the Ni_3Ga alloy after preliminary tests featuring films with 1:1, 3:1, and 5:3 stoichiometries indicated that, in our hands, the 3:1 variant was the most successful at reducing CO_2 to CO, a possible intermediate leading to more highly reduced products.[26] We show that Ni_3Ga thin films exhibit different surface morphologies and electrocatalytic behaviors when deposited on different carbon solid supports. Furthermore, we find that unsupported, bulk Ni_3Ga, though unreactive toward CO_2, is a modest CO reduction catalyst capable of generating MeOH, and that introducing a carbon solid support alters this behavior to make the material more active toward the CO_2 reactant. We attribute these characteristics to a catalyst deposition effect exerted by the carbon solid support, whereby the support dictates thin film morphology and gives the film a different surface composition compared to unsupported materials. We use this understanding to create an electrochemical system, featuring tandem Ni_3Ga electrodes of different morphologies, which improves the performance of the electrochemical cell in reducing CO_2 to methanol.

Experimental

Materials.—Nickel(II) nitrate hexahydrate (99.999%), gallium(III) nitrate hydrate (99.9%), nickel powder (<150 μm, 99.995%), gallium (99.99%), nickel(0) bis(1,5-cyclooctadiene) ($Ni(cod)_2$), gallium(III) acetylacetonate ($Ga(acac)_3$; 99.99%), K_2SO_4 (≥99.0%), 1,4-dioxane (99.8%), 1-octadecene (90%), toluene (99.8%), isopropanol (≥99.7%), $^{13}CO_2$, and C_2H_6 were purchased from Sigma-Aldrich and used as received. Tanks of Ar, N_2, CO_2, CO, 95% Ar/5% H_2, and 50% CO/50% H_2 gases and mixtures were obtained from AirGas. Glassy carbon (GLAS11; 25 × 25 × 3 mm) and highly oriented pyrolytic graphite (HOPG; Grade SPI-3; 10 × 10 × 1 mm) plates were purchased from Structure Probe Inc., and glassy carbon pieces were cut in half lengthwise prior to use in electrochemical experiments. Glassy carbon and HOPG electrode plates were cleaned using wet 1.0-μm alumina on a polishing pad and Scotch brand tape, respectively. Reticulated vitreous carbon (RVC) foam was

*Electrochemical Society Member.
zE-mail: bocarsly@princeton.edu

acquired from ERG Materials and Aerospace, Corp., and cut into pieces approximately 20 × 0.5 × 0.5 cm in size before use. Copper tape was obtained from Structure Probe Inc. and conducting silver epoxy and Loctite Hysol insulating epoxies were purchased from Epo-Tek and Grainger. Bottles of MeOH (>99.9%) and formic acid (≥ 98%), used to create standard curves, were purchased from Sigma-Aldrich and diluted to known concentrations prior to examination.

Synthesis of Ni_3Ga films on solid supports.—Ni_3Ga films on HOPG were synthesized according to the method reported by Torelli et al.[26] This synthetic method was adapted to achieve Ni_3Ga films on glassy carbon and RVC foams. Briefly, aqueous solutions of 0.052 M nickel(II) nitrate hexahydrate and 0.036 M gallium(III) nitrate hydrate were mixed in a 3:1 ratio, and 0.5-mL samples of the combined solution were drop-casted onto either glassy carbon plates or RVC foam pieces that had been heated to 150°C on a hot plate. The solid supports were left on the hot plate until the water from the solution had evaporated. The solid supports were placed in alumina boats and loaded into a Carbolite Quartz Tube Furnace under 95% Ar/5% H_2 gas flow. The furnace was ramped at a rate of 3°C/min to 700°C, where it rested for 5 h. Then, the furnace was returned to room temperature at a rate of –3°C/min. Upon removal from the furnace, Ni_3Ga films appeared tan in color and adhered to the surface of the HOPG and glassy carbon solid supports and both on the surface and within the pores of the RVC foam.

Synthesis of bulk Ni_3Ga.—Polycrystalline samples of Ni_3Ga were prepared by an initial solid-state reaction method using high-purity elemental nickel and gallium. Stoichiometric amounts of starting materials were placed into quartz tubes and sealed under vacuum. The tubes were heated to 1000°C at a rate of 3°C/min and held at that temperature for 12 h. The samples were then cooled by quenching in room temperature water. The resulting polycrystalline chunks were loaded onto a water-cooled copper hearth and arc-melted under Ar atmosphere. Each sample was turned over in the Ar-filled chamber and re-melted twice to ensure homogeneity in the polycrystalline spheres. No mass loss occurred during this melting treatment.

Synthesis of Ni_3Ga nanoparticles.—The synthesis of Ni_3Ga nanoparticles was adapted from Kirkeminde et al.[28,29] First, 16 mL of 1-octadecene (ODE) was added to a three-neck flask equipped with a condenser and attached to both a standard Schlenk line and a side-arm adapter connected to a secondary bubbler; the solution was purged with Ar. A separate flask was loaded with 0.5 mmol $Ga(acac)_3$ and 3 mL ODE, purged with Ar for 15 min, and heated to 85°C. In a third flask, 0.5 mmol $Ni(cod)_2$ was dissolved in 5 mL toluene under N_2 atmosphere. The temperature of the original three-neck flask was adjusted to 310°C. The system was set such that Ar gas flowed out of the secondary bubbler, and the two metal solutions were simultaneously and slowly injected into the three-neck flask to ensure complete evaporation and escape of the toluene vapor. The reaction was left to stir under reflux at 310°C for 1 h, after which time a black precipitate was collected and washed with 50:50 toluene:acetone and then centrifuged at 5500 RPM for 15 min; the supernatant was discarded. The washing procedure was repeated twice, and the product was collected in acetone and dried under vacuum. Finally, the collected material was annealed at 550°C for 12 h in a Carbolite Quartz Tube Furnace under 95% Ar/5% H_2 gas flow.

Materials characterization.—All Ni_3Ga samples, apart from RVC-plated films, were analyzed by powder X-ray diffraction using a Bruker D8 Advance Diffractometer Eco with CuKα radiation and a LynxEye-XE detector. The scan parameters were 0.02°/step with 0.085 s/step, resulting in a total scan time of 8 min. XRD patterns of thin films on glassy carbon and HOPG were obtained both while the film was affixed to the solid support and after the film had been scraped from the solid support. Both patterns yielded the same Ni_3Ga peaks, while the scraped versions exhibited significantly less background carbon intrusion. Bulk Ni_3Ga was ground to a powder prior to examination by XRD.

A FEI XL30 FEG-SEM equipped with EVEX EDS detector was used to examine the morphology and composition of all materials before and after electrochemical experimentation. SEM images and EDX spectra were obtained using a 5 or 10 keV electron beam with a 10–15 mm working distance. Nanoscale images of Ni_3Ga nanoparticles were achieved using a FEI CM200 FEG-TEM. A ThermoFisher K-Alpha X-Ray Photoelectron Spectrometer was used to collect surface compositional data. These data were obtained using 20 eV pass energy and 50 ms dwell time, and analysis was performed using Thermo Scientific Avantage Data System and CasaXPS software.

Electrode preparation and electrochemical experimentation.—Electrodes were prepared using slightly different strategies depending on the form of the alloy. HOPG, glassy carbon, and RVC foam electrodes were prepared by affixing copper tape to the solid support and then separately preparing a support "holder" comprised of an alligator clip attached to a copper wire, which was threaded through a glass tube sealed on both ends using insulating epoxy. The alligator clip was then used to hold the solid support of interest. In all experiments, care was taken to ensure that the copper tape was not exposed to the electrolyte. Control experiments were carried out to confirm that the copper tape was not inadvertently acting as a CO_2 reduction catalyst. Additionally, copper was not detected on electrode surfaces by post-electrolysis XPS analysis.

Bulk Ni_3Ga electrodes were created by sanding a polycrystalline sphere of the alloy using progressively finer sandpapers to achieve a round, flat surface having a diameter of 2–3 mm. The surface was then polished using 1.0-μm diamond paste. Copper wire was attached to the back of the pellet (i.e., the side opposite the flat, polished surface) using conducting silver epoxy, while the length of the wire was fed through a glass tube. As previously described, both ends of the glass tube were sealed with insulating epoxy. The insulating epoxy was used to cover any exposed conducting silver epoxy as well as any non-polished surfaces of the Ni_3Ga pellet.

Working electrodes containing the Ni_3Ga nanoparticles were prepared using a drop-casting procedure established by White.[30] To begin, 2 mg/mL of nanoparticles were suspended in isopropanol and sonicated for 30 min. Then, 30 μL of 15 wt% LIQUion Solution LQ-1115 1100EW (Ion Power) was added, and the solution was sonicated for an additional 60 min to form a black ink. The mixture was drop-casted onto glassy carbon or RVC pre-heated to 120°C, and the liquid was permitted to evaporate.

Cyclic voltammetry and bulk electrolysis experiments were performed using CH Instruments 760 and 1140 potentiostats. Cyclic voltammetry experiments utilized a three-neck round-bottom flask as the electrochemical cell, which was equipped with a Ni_3Ga working electrode alongside a Ag/AgCl reference and a Pt mesh counter electrode. An aqueous solution of 0.1 M K_2SO_4 was used as the electrolyte. After thorough CO_2 purging, the pH of the electrolyte was ∼4.5, therefore during cyclic voltammetry under Ar or CO the pH was adjusted to this value with 0.01 M H_2SO_4. The same electrolyte solution was used in bulk electrolysis experiments featuring custom electrolysis cells with gastight ports for the previously listed electrodes. During bulk electrolysis, the Pt mesh counter electrode was held in a fritted gas dispersion tube and the electrolysis solution was stirred. Cyclic voltammetry and electrolysis solutions were purged with CO_2, CO, or Ar for 20 min prior to experimental or control trials; experiments featuring $^{13}CO_2$ starting material were not completely purged and therefore witnessed minor amounts of $^{12}CO_2$ intrusion. pH dependence experiments utilized K_2SO_4 electrolyte buffered with $KHCO_3$ (to achieve CO_2-purged pH values > 4.5) or adjusted with 0.01 M H_2SO_4 (to achieve CO_2-purged pHs down to 3.5). In general, bulk electrolysis experiments were performed until 30 (HOPG, bulk) or 60 C (glassy carbon, RVC foam) of charge had passed, and CO_2 was supplied to the systems throughout the experiment. Bulk solution

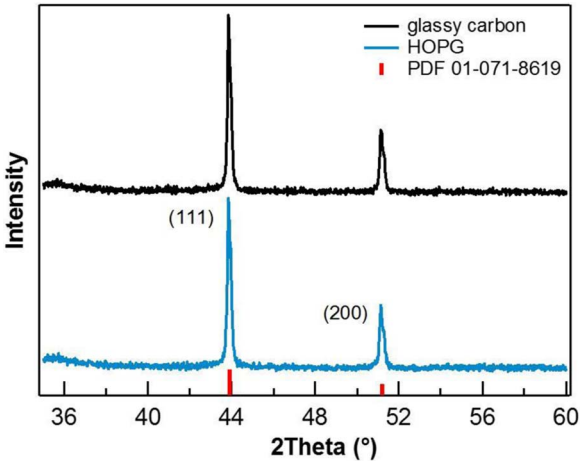

Figure 1. Powder XRD patterns of Ni_3Ga thin films synthesized on HOPG (blue) and glassy carbon (black) referenced to PDF 01-071-8619 (red).

pH was measured before and after each electrolysis experiment to confirm that pH changes were negligible (i.e., $\leq$ 0.2 pH units).

Product analysis.—During and/or after bulk electrolysis experiments, the electrolysis cell was sampled for liquid and gaseous products. To sample the solution, ^{1}H-NMR was performed with a Bruker Avance III 500 MHz NMR Spectrometer and cryoprobe detector after combining 530 μL of the experimental electrolyte with 60 μL D_2O and 10 μL 1,4-dioxane (10mM; internal standard). A custom water suppression method was employed. Liquid products were quantified using 5-point calibration curves.

The headspace of the electrolysis cell was sampled using gas chromatography. CO was detected using a HP6890 Gas Chromatograph and TCD with a Molsieve 5A PLOT capillary column (Agilent) running He as the flow gas for a 5-min, 60°C isothermal method. C_2H_6 was detected using the same instrument running a 5-min, 150°C isothermal method after the electrolysis cell was subjected to an acetone/ice bath for 10 min to minimize the occurrence of water in the headspace. H_2 was sampled using a 7-min isotherm at 80°C on an SRI 8610C Gas Chromatograph and TCD with a Molsieve column and Ar flow. Gaseous products were quantified using 30-point calibration curves having $R^2 \geq 0.99$. After bulk electrolyses using $^{13}CO_2$, a headspace sample was collected in a gas cell terminated by KBr plates and subsequently examined using a Nicolet 730 FT-IR Spectrometer with 1 cm^{-1} resolution.

Faradaic efficiencies were calculated based on the total charge passed during each experiment, as well as the product quantities determined by gas- and liquid-phase sampling. Catalytic efficiency parameters (ξ) were calculated based on the following equation developed by Pander and Bocarsly:[31]

$$\text{Catalytic efficiency parameter, } \xi\ (\%) = \frac{\text{Faradaic efficiency}}{\left(1 - \frac{\text{overpotential}}{E^{\circ\prime}_{\text{product}}}\right)} \times 100 \quad [1]$$

Results and Discussion

Ni_3Ga thin films on HOPG.—To evaluate differences in Ni_3Ga-catalyzed CO_2 electroreduction based on the solid support employed, several carbon-based electrode materials were selected on which to synthesize Ni_3Ga thin films. HOPG was chosen to emulate the original report of Ni-Ga thin film-facilitated CO_2 reduction, and the film was obtained by drop-casting metal nitrate solutions onto the support before reducing to the metallic state in a tube furnace.[26] The composition of the resulting material was examined by powder X-ray diffraction (XRD) as shown in Figure 1, which confirmed that Ni_3Ga having a face-centered cubic lattice had been synthesized. Cyclic voltammetry

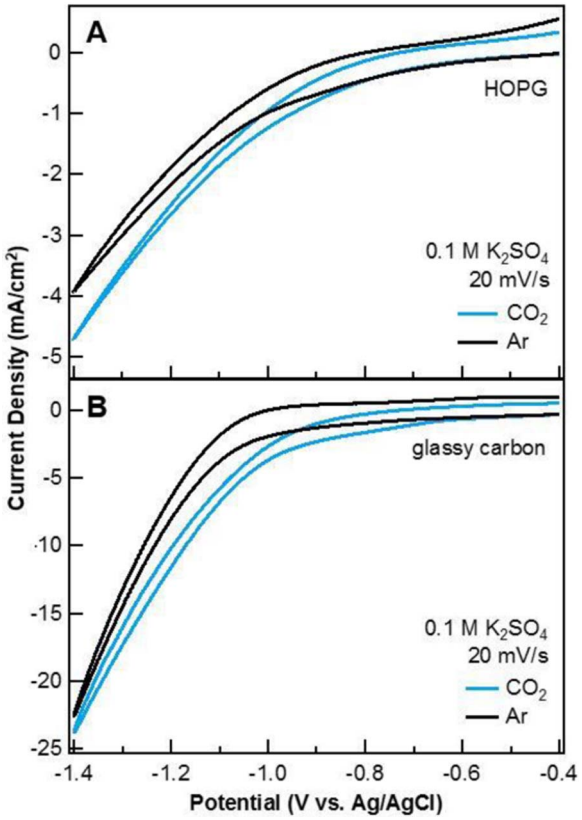

Figure 2. Cyclic voltammograms obtained using Ni_3Ga thin films on (A) HOPG and (B) glassy carbon solid supports under CO_2 versus Ar atmosphere. Data were collected using a Pt mesh counter electrode and 0.1 M K_2SO_4 electrolyte (pH 4.5 after CO_2 saturation; Ar scans adjusted with H_2SO_4) at a scan rate of 20 mV/s.

with Ni_3Ga on HOPG exhibited a current enhancement under CO_2 atmosphere with an onset around –0.8 V vs. Ag/AgCl (Figure 2A). Here and throughout this work, current density presented in cyclic voltammograms is calculated based on geometric surface area. Subsequent bulk electrolysis experiments were performed in 0.1 M K_2SO_4 having an initial pH ~6.8; however, CO_2 saturation caused the pH to drop to 4.5 and remain largely unchanged during electrolysis (i.e., bulk pH changed by $\leq$ 0.2 pH unit). K_2SO_4 was chosen as a pH-neutral electrolyte with the anticipation of performing pH dependence studies by buffering with $KHCO_3$, since proton availability has been shown, especially in copper-mediated CO_2 reduction, to drastically impact product selectivity.[32,33]

Ni_3Ga/HOPG electrodes were subjected to bulk electrolysis using a Pt mesh counter electrode and an applied potential of –1.38 V vs. Ag/AgCl, as reported by Torelli et al.[26] This resulted in the production of C_2H_6 with 0.10 ± 0.01% faradaic efficiency ($\xi = 0.026\%$) as the only carbon-containing product observed. The rest of the charge contributed to H_2 generation (98 ± 1%), which was visible by rapid bubbling at the electrode surface during experimentation; faradaic efficiencies for both products were pH-independent. Control experiments which sealed the edges of the HOPG electrode, where most edge planes are expected to exist, with insulating epoxy suggested that the carbon product was likely generated on the basal plane-confined Ni_3Ga film. This result accords with the findings of Torelli et al. who, on HOPG, found Ni-Ga films to generate small amounts C_2H_6, as well as CH_4 and C_2H_4. Their bulk electrolysis and cyclic voltammetry results also suggest that the mechanism of CO_2 reduction on this material passes through a CO intermediate,[26] which we confirmed by using CO as a feedstock (in place of CO_2) after adjusting the bulk pH to 4.5, which resulted in C_2H_6 production at a slightly higher faradaic efficiency of 0.31 ± 0.02% ($\xi = 0.042\%$). Based on this result, we

agree with Torelli's conclusion that CO is a key reaction intermediate in the Ni_3Ga/HOPG system.

Ni_3Ga thin films on glassy carbon.—While HOPG is comprised of layered graphene sheets,[34] glassy carbon is made up of an sp^2 network resembling distorted fullerenes,[35] so choice of glassy carbon as a solid support provided a morphologically different material having an electronic structure related and in some ways similar to that of HOPG.[36,37] The Ni_3Ga thin film on glassy carbon, whose XRD pattern is displayed in Figure 1, produced cyclic voltammograms as shown in Figure 2B. Like HOPG-plated films, current enhancement is observed under CO_2 atmosphere, but the onset of this enhancement begins at a more positive potential around –0.6 V vs. Ag/AgCl. Electrolysis experiments were therefore undertaken to analyze product distribution.

When bulk electrolysis was performed using Ni_3Ga films on glassy carbon, a difference in reactivity toward CO_2 was immediately evident. No multiple-carbon products were formed, and the major product of the reaction, at –1.38 V vs. Ag/AgCl and pH 4.5, was CO with a faradaic efficiency of 11.2 ± 0.7% (ξ = 5.0%). Formate and MeOH were also formed in the liquid phase in small amounts, having faradaic efficiencies of 0.23 ± 0.05% and 0.06 ± 0.01% (ξ = 0.084 and 0.020%), respectively. As this is the first report of Ni_3Ga on glassy carbon electrocatalysis, product distribution based on bulk solution pH (using K_2SO_4 buffered with $KHCO_3$) was undertaken. This study (see Figure S1) motivated the selection of pH = 4.5 as optimal for electrolysis experiments. Control experiments using $^{13}CO_2$ as the reactant confirmed that all three products were generated from CO_2 (Figure S2). Based on the HOPG experiments, it was expected that using a CO feedstock with the glassy carbon-plated film would result in similarly small amounts of formate and MeOH, but instead only H_2 was observed, suggesting that a different—or at least a second—CO_2 reduction pathway independent of CO is possible when Ni_3Ga is plated on glassy carbon.

To determine what differences existed in the HOPG- versus glassy carbon-plated films that could help explain the dissimilar product distributions and mechanistic pathways, the two materials were characterized as follows. The powder XRD pattern of Ni_3Ga/glassy carbon indicated no difference in the alloy's crystalline plane preference when compared to the HOPG variant (Figure 1). Energy dispersive X-ray spectroscopy (EDX) analysis suggested similar metal stoichiometries and oxygen content regardless of solid support identity. However, examination by scanning electron microscopy (SEM) demonstrated that the morphology of the thin film depends on the solid support material. As shown in Figures 3A, 3B, the Ni_3Ga film on HOPG is a discontinuous array of microparticles having rough or layered surfaces, while the same film on glassy carbon is comprised of uniform platelets with relatively flat surfaces. As discussed previously, dependence of morphology[12,13] or other material properties[14,15] on solid support identity, particularly considering cases in which materials are grown directly onto a solid support, is not unprecedented. To further test this concept, a third carbon support material, reticulated vitreous carbon (RVC), was examined. While chemically equivalent to glassy carbon, RVC exhibits a porous macrostructure and high surface area.

Ni_3Ga thin films on RVC.—Ni_3Ga thin films were synthesized on 80 ppi RVC foam and analyzed by EDX (rather than XRD, which would have required destruction of the film and support) to confirm stoichiometry (Figure S3) and SEM to examine morphology. SEM imaging (Figure 3C) revealed that the morphology of the RVC-plated film resembled that achieved on glassy carbon. Namely, the film was comprised of uniform platelets distributed across the struts of the solid support; the platelets, while flat, appeared slightly rougher than their glassy carbon-deposited counterparts. This similar morphology may be attributed to the fact that carbon foams and glassy carbon are microstructurally comparable and electronically identical vitreous materials.[38,39]

Following cyclic voltammetry experiments (Figure S4), bulk electrolysis was performed at –1.38 V vs. Ag/AgCl, and it was found that

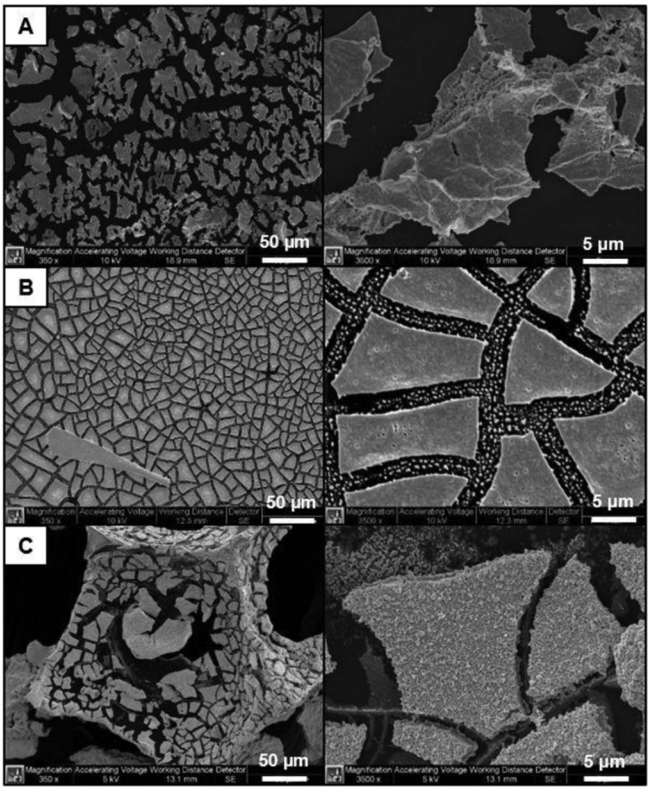

Figure 3. SEM images of Ni_3Ga thin films synthesized on (A) HOPG, (B) glassy carbon, and (C) 80 ppi RVC foam solid supports at low (left) and high (right) magnification. While HOPG-plated films are comprised of layered microparticles, glassy carbon and RVC variants consist of relatively uniform platelets distributed across the surface.

the RVC-plated films generated CO, formate, and MeOH at faradaic efficiencies of 26 ± 2%, 1.0 ± 0.1%, and 0.10 ± 0.02% (ξ = 12, 0.37, and 0.033%), respectively. As in all prior experiments, bulk pH changes were negligible during electrolysis. As displayed in Figure 4, RVC-derived products are the same as those achieved on glassy carbon, and the products are generated in the same ratio independent of the solid support. While maintaining the same product branching ratio, the faradaic efficiencies achieved on RVC are approximately double the values obtained on glassy carbon. The pH dependence plot for RVC (Figure S1), when compared to glassy carbon, tends to follow

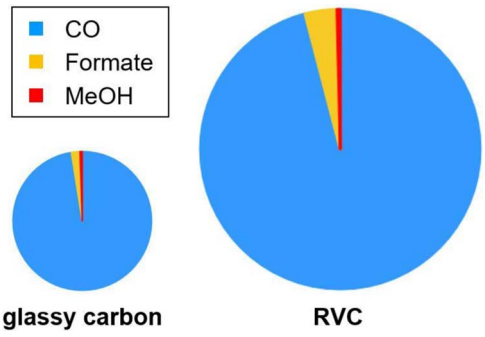

Figure 4. CO_2 product distribution achieved using Ni_3Ga films deposited on vitreous carbon solid supports. Relative ratios of CO, formate, and MeOH are generally the same for glassy carbon and RVC-plated films, while the faradaic efficiencies from RVC were approximately double those obtained from glassy carbon (indicated by the relative sizes of the circle plots). Electrolysis experiments were conducted at –1.38 V vs. Ag/AgCl using a Pt mesh counter electrode and 0.1 M K_2SO_4 electrolyte saturated with CO_2 (pH 4.5).

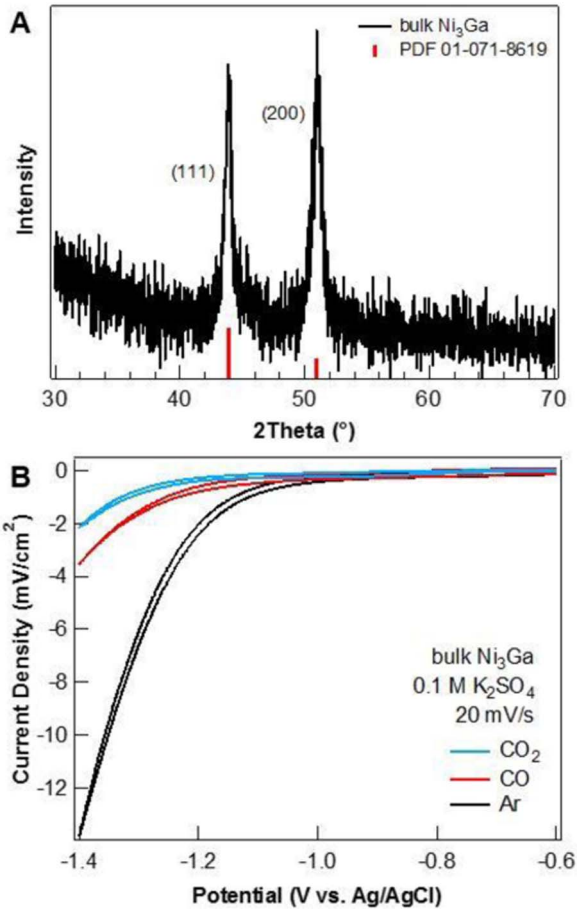

Figure 5. Material and electrochemical characterization of bulk Ni_3Ga electrodes. (A) Powder XRD pattern of bulk Ni_3Ga (black) referenced to PDF 01-071-8619 (red). (B) Cyclic voltammograms obtained using a bulk Ni_3Ga working electrode under CO_2, CO, or Ar saturation. Data were collected using a Pt mesh counter electrode and 0.1 M K_2SO_4 electrolyte (pH 4.5 after CO_2 saturation; Ar and CO scans adjusted with H_2SO_4) at a scan rate of 20 mV/s.

the same trend. Thus, the facilitated chemistry is equivalent on the two catalysts, despite one form being more charge-efficient than the other. The remainder of the charge passed in the Ni_3Ga/RVC electrolyses contributed to H_2 evolution (71 ± 3%), as determined by GC analysis. Like glassy carbon-deposited Ni_3Ga, RVC-plated films generated either no or negligible quantities of formate and MeOH when supplied with CO in place of CO_2 as a feedstock gas, suggesting that the films generated on vitreous carbon solid supports, rather than HOPG, reduce CO_2 using a similar reaction mechanism.

Polycrystalline, unsupported Ni_3Ga.—Considering that two very different sets of products could be achieved using the same bimetallic alloy material on different solid supports, an unsupported, bulk Ni_3Ga alloy was also investigated. Following powder XRD characterization of the freestanding alloy (Figure 5A), electrodes were used in cyclic voltammetry experiments in 0.1 M K_2SO_4 under Ar and CO_2 saturation (pH 4.5 in both cases). Unlike the supported systems, and as shown in Figure 5B, current density decreased under CO_2 compared to Ar when using unsupported Ni_3Ga electrodes, suggesting that H_2 evolution was disrupted by CO_2 at or near the electrode surface.[40] Bulk electrolysis experiments after CO_2 purging appeared to generate trace or no liquid products, and faradaic efficiencies of only 0.91 ± 0.05% ($\xi = 0.40\%$) for CO were achieved across a range of applied potentials. Besides H_2, quantified at nearly 100% faradaic efficiency, no other gaseous products were detected. Thus, bulk Ni_3Ga is not active toward CO_2 electroreduction.

Bulk Ni_3Ga electrodes were also evaluated using CO as the reactant. At an applied potential of –1.38 V vs. Ag/AgCl (pH 4.5), MeOH was detected by ^{1}H-NMR and exhibited a faradaic efficiency of 2.1 ± 0.4% ($\xi = 0.20\%$). ^{1}H-NMR following electrolysis experiments using ^{13}CO starting material confirmed that the product was derived from CO (Figure S5). Furthermore, cyclic voltammetry performed under CO saturation exhibits a higher current density than that achieved using CO_2 (Figure 5B). Thus, it is evident that the catalytic activity of this alloy material can be adjusted using a carbon-based solid support, transforming a material with modest reactivity toward CO and no catalytic activity toward CO_2 into a material that is capable of reducing CO_2.

Ni_3Ga nanoparticles.—Since the results reported here indicate that vitreous carbon-supported Ni_3Ga favors CO generation from CO_2 and unsupported Ni_3Ga is specific for the reduction of CO, it was hypothesized that putting unsupported Ni_3Ga onto a vitreous carbon solid support might improve MeOH formation from CO_2. To test this idea, unsupported Ni_3Ga nanoparticles were synthesized and then applied to a carbon support for electrochemical analysis. Ni_3Ga nanoparticles were synthesized using a procedure adapted from Kirkeminde et al.[28,29] As shown in Figures 6A, 6B, powder XRD of the annealed nanoparticles confirmed the desired stoichiometry and, along with transmission electron microscopy (TEM) imaging, determined that the nanoparticles were 10–20 nm in diameter. The nanoparticles were suspended in Nafion solution (1100EW) and drop-casted onto a glassy carbon or RVC electrode. A representative SEM image of Ni_3Ga nanoparticles on glassy carbon solid support is displayed in Figure S6.

Using identical conditions to those previously described, cyclic voltammograms obtained from glassy carbon-bound nanoparticles more closely resembled those recorded for the bulk Ni_3Ga electrodes than the thin films, as higher current was observed leading into the proton reduction wave when the atmosphere was saturated with Ar than CO_2 (Figure 6C). Accordingly, bulk electrolysis performed at a variety of potentials failed to generate any liquid CO_2 reduction products. Though CO was detected at < 1% faradaic efficiency, the majority of charge passed contributed to H_2 evolution, as would be predicted based on cyclic voltammetry data resembling bulk Ni_3Ga. Therefore, simply having Ni_3Ga supported on vitreous carbon is not sufficient to activate the CO_2 reduction channel.

These data show that the application of Ni_3Ga onto glassy carbon after the alloy's synthesis does not induce CO generation comparable to Ni_3Ga grown directly onto the solid support. This suggests that the solid support's role in altering CO_2 reduction products is indirect; the support does not play a chemical role during CO_2 electroreduction. This assertion is further supported by the fact that CO generation still occurs when CO_2 reduction is performed using a glassy carbon-bound Ni_3Ga film after coating the solid support's exposed surfaces (i.e., where the Ni_3Ga thin film is not situated) with insulating epoxy.

Ni_3Ga tandem-electrode system.—To test the finding that different morphologies of Ni_3Ga differ in their reactivity toward CO_2, two types of Ni_3Ga electrodes were employed in the same electrochemical cell. The first electrode was comprised of a Ni_3Ga morphology specific for generating CO from CO_2, while the second electrode morphology was selected for its ability to generate organic products from CO. If the hypothesis is correct that the first morphology is a relatively efficient CO_2-reducer and the second morphology performs CO reduction, then this setup would produce CO from CO_2 in situ at the first electrode's surface and provide a higher effective concentration of CO at the second electrode's surface (i.e., as it is generated) for use in MeOH generation.

As the best CO generator of the Ni_3Ga thin films, the 80 ppi RVC-plated variant was selected as the first working electrode, and a bulk Ni_3Ga disk electrode was chosen as the second, since this material does not react with CO_2 (schematic representation in Figure S7). Electrolysis experiments were then performed at –1.38 V vs. Ag/AgCl in CO_2-saturated, pH 4.5 K_2SO_4 electrolyte using the RVC and bulk

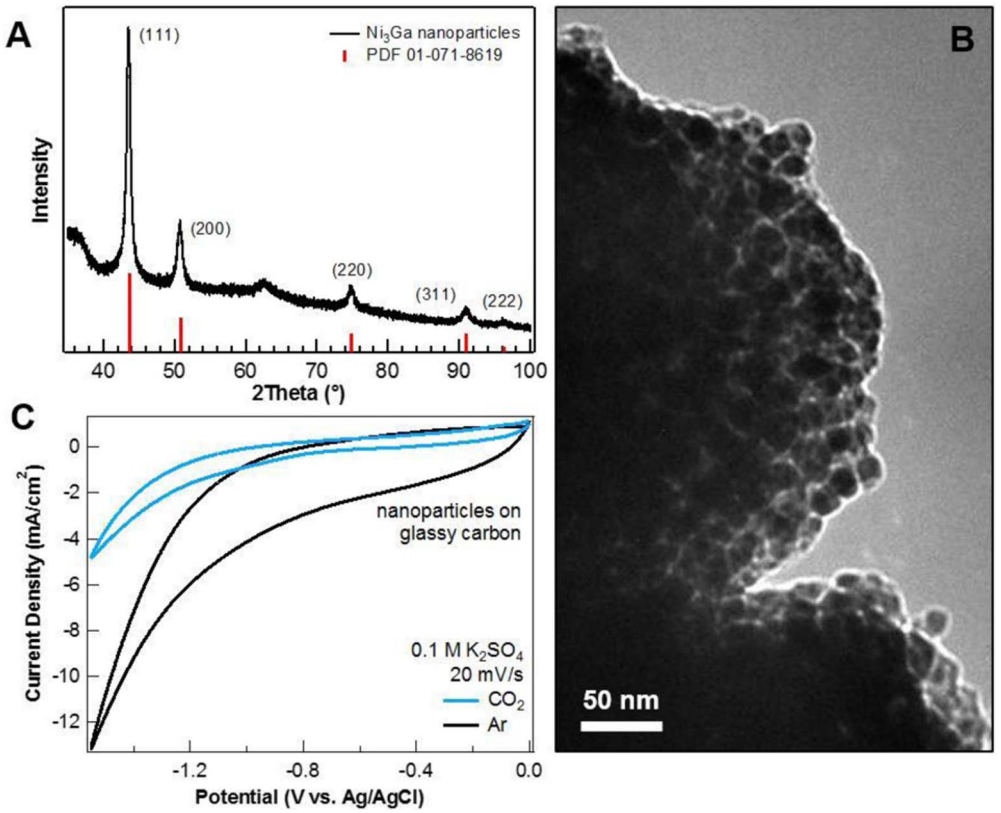

Figure 6. Material and electrochemical characterization of annealed Ni_3Ga nanoparticles. (A) Powder XRD pattern of Ni_3Ga nanoparticles (black) referenced to PDF 01-071-8619 (red). The broad peak at 61.5° is attributed to NiO. (B) TEM image of a nanoparticle cluster, indicating that average particle size is 10–20 nm. (C) Cyclic voltammograms obtained using Ni_3Ga nanoparticles drop-casted onto glassy carbon under CO_2 or Ar saturation. Data were collected using a Pt mesh counter electrode and 0.1 M K_2SO_4 electrolyte (pH 4.5 after CO_2 saturation; Ar and CO scans adjusted with H_2SO_4) at a scan rate of 20 mV/s.

electrodes either in series or in tandem. In series experiments, the Ni_3Ga film on RVC was situated as the first operational working electrode. As expected, CO was generated at a faradaic efficiency around 20%. After a few hundred micromoles of CO had been generated, the experiment was stopped and the working electrode was switched to the bulk Ni_3Ga disk. The second electrolysis was run until at least 4 C of charge had passed, at which time a noticeable decrease in headspace CO was recorded. Analysis of the electrolyte indicated that MeOH was generated from CO at a faradaic efficiency of $7.1 \pm 0.1\%$ ($\xi = 0.66\%$). In tandem-use experiments, RVC and bulk electrodes were operated simultaneously, CO was once again detected in the headspace, and electrolyte analysis revealed that MeOH was generated from CO at $13.2 \pm 0.4\%$ faradaic efficiency ($\xi = 1.2\%$).

Figure 7 compares the faradaic efficiencies for MeOH achieved using an external CO purge with those calculated when CO was generated in situ during series or tandem Ni_3Ga-mediated experiments. MeOH faradaic efficiencies achieved when operating the RVC and bulk electrodes in tandem were nearly double those noted when the electrodes were used in series. These data make sense, as operating both electrodes simultaneously lowers the ability of Ni_3Ga/RVC-generated CO, which exhibits poor solubility in water, to escape to the headspace before being further reduced by bulk Ni_3Ga. Control trials indicated that negligible quantities of MeOH were formed during the RVC stage of in-series electrolysis, confirming that CO was in fact converted to MeOH on bulk Ni_3Ga.

Influence of solid support on electrocatalysis via morphology.— Having determined the electrochemical CO_2 reactivity profiles of supported and unsupported Ni_3Ga, experiments were undertaken to understand how variation in carbon support materials induces Ni_3Ga, a material whose native activity is modest toward CO reduction, to be active toward CO_2. Our experiments featuring Ni_3Ga nanoparticles drop-casted onto glassy carbon after their synthesis suggest that the impact of a carbon solid support in altering electrochemical behavior is indirect (i.e., the support is not playing a chemical role during electrolysis). Instead, the carbon support must affect the material properties of the film, perhaps having its effect during synthesis of the Ni_3Ga

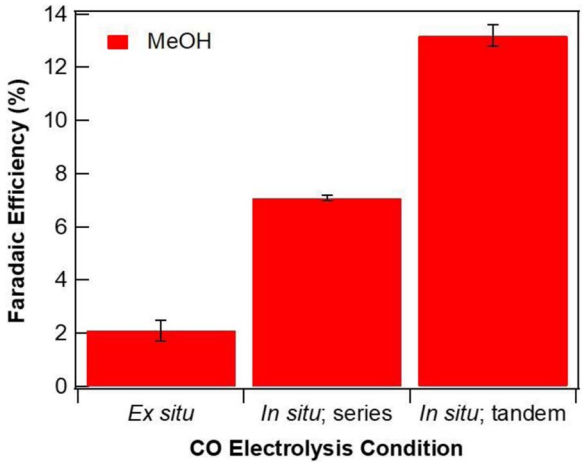

Figure 7. Faradaic efficiencies for MeOH achieved using bulk Ni_3Ga electrodes exposed to CO in solution. CO was either supplied to the system prior to electrolysis (ex situ) or generated from CO_2 internally by the system using a Ni_3Ga thin film on 80 ppi RVC (in situ). In situ experiments either operated the RVC and bulk electrodes in series or in tandem. Electrolysis experiments were conducted at –1.38 V vs. Ag/AgCl using a Pt mesh counter electrode and 0.1 M K_2SO_4 electrolyte.

Table I. Surface compositions of bulk Ni_3Ga (i.e., unsupported) and Ni_3Ga thin films synthesized on HOPG and glassy carbon solid supports.

	Ni (atomic %)	Ga (atomic %)
Bulk Ni_3Ga	73 ± 2	27 ± 2
Ni_3Ga/HOPG	17 ± 2	83 ± 2
Ni_3Ga/glassy carbon	28 ± 4	72 ± 4

thin films in such a way that CO_2 reduction behavior is impacted later on. During synthesis, the carbon solid support is not instrumental in the reduction of the Ni and Ga ions to their metallic, alloyed state, because use of alternative, non-carbon solid supports still results in generation of a Ni_3Ga film (i.e., Si wafer, ZnSe disk, and Ni sheet were all evaluated). Therefore, the solid support's impact during synthesis must manifest in the structures of the films themselves. Powder XRD and EDX confirm that the bulk composition of the Ni_3Ga films studied here are identical whether the films are synthesized on HOPG or glassy carbon. However, SEM imaging demonstrates that surface morphologies distinctly depend on the identity of the carbon solid support. It was therefore hypothesized that the surfaces of differently synthesized Ni_3Ga alloys might be further differentiated based on atomic composition.

To answer this question, X-ray photoelectron spectroscopy (XPS) was performed with Ni_3Ga films supported on HOPG and glassy carbon, as well as unsupported bulk Ni_3Ga for comparison. The atomic percentages of surface Ni and Ga derived from bulk Ni_3Ga (i.e., unsupported), Ni_3Ga/HOPG, and Ni_3Ga/glassy carbon are listed in Table I. XPS of bulk Ni_3Ga indicates that the material's surface is comprised of a nearly exact 3:1 ratio of Ni and Ga, which has been reported as a relatively poor CO_2-reducing stoichiometry.[26,41,42] On the other hand, the surfaces of Ni_3Ga thin films synthesized on HOPG and glassy carbon are both Ga-rich, despite the fact that the bulk compositions of these films exhibit their namesake 3:1 Ni:Ga stoichiometry (Figure 1). Considering that heterogeneous CO_2 reduction occurs at the electrode's surface, we suggest that the different surface stoichiometries achieved on bulk versus thin film Ni_3Ga are instrumental in determining the materials' reactivities toward CO_2 in solution. Namely, unsupported Ni_3Ga is unreactive toward aqueous CO_2, while films on glassy carbon or HOPG, exhibiting the same surface composition, are active CO_2 reduction catalysts. Comparing the XPS data for Ni_3Ga films on HOPG and glassy carbon, shown in Figure S8, it is evident that the Ni and Ga present on both surfaces are mixtures of metals and metal oxides. As listed in Table S1, the relative quantities of surface metal and metal oxides making up Ni_3Ga films on HOPG and glassy carbon are comparable, further confirming that surface composition of thin films is not dependent on choice of solid support.

Finally, while differences in electrochemically active surface area, and thus carbon coverage by the Ni_3Ga thin films, could theoretically explain the differing activities, particularly when comparing product identity profiles observed on HOPG versus vitreous materials, measurements of surface coverage do not support this possibility. Based on SEM data, the percentages of carbon support covered by Ni_3Ga on HOPG, glassy carbon, and RVC were approximately 48%, 42%, and 17%, respectively. RVC exhibited the lowest surface coverage and, as such, the highest amount of exposed carbon, so it was important to determine whether this exposed carbon could provide beneficial effects during CO_2 electroreduction. Experiments analyzing ferrocyanide/ferricyanide, hydroquinone/benzoquinone, and several other common redox couples indicated that vitreous carbon materials (i.e., both glassy carbon and RVC) lost their ability to facilitate these redox reactions after heat-treatment, likely due to loss of native surface functionalities in the high-temperature, slightly reducing furnace conditions.[43–45] Thus, synergistic effects between drop-casted Ni_3Ga and these carbon supports are unlikely during electrochemical experimentation. Furthermore, the product distribution differences observed on HOPG and vitreous carbon supports cannot be explained by differences in carbon surface coverage, as the percentage of carbon covered by thin film is generally equivalent in the HOPG and glassy carbon cases. Thus, carbon coverages and active surface areas must not be the reason for differing electrochemical outcomes by carbon-supported Ni_3Ga.

Table II. Summary of electrolysis products generated by five morphologies of Ni_3Ga exposed to either CO_2 or CO in aqueous solution. Electrolysis experiments were performed at –1.38 V vs. Ag/AgCl in 0.1 M K_2SO_4 (pH 4.5).

	CO_2 feedstock	CO feedstock
thin film/HOPG	C_2H_6, H_2	C_2H_6, H_2
thin film/glassy carbon	CO, Formate, MeOH, H_2	H_2
thin film/RVC	CO, Formate, MeOH, H_2	H_2
unsupported bulk	H_2	MeOH
nanoparticles	H_2	H_2

Conclusions

The only remaining—and glaring—difference in Ni_3Ga thin film surfaces having dissimilar carbon supports is their surface morphologies. Recalling Figure 3, SEM imaging shows that Ni_3Ga on HOPG has a significantly rougher surface than Ni_3Ga on glassy carbon, whose surface is flatter and more uniform. Due to the microstructuring and high surface area of Ni_3Ga/HOPG, one might imagine that surface-bound reduction intermediates would exist in close proximity to one another, facilitating C–C bond formation on HOPG-deposited films. This sort of intermediate binding and coupling would, based on geometry, not be promoted on flat Ni_3Ga/glassy carbon surfaces, which instead favor generation of one-carbon products. We suggest that these morphological differences contribute to the product discrimination observed for Ni_3Ga thin films on different carbon solid supports.

By synthesizing and testing various forms of Ni_3Ga alloy catalysts, we have shown that, like copper electrode systems, significant morphological and solid support influences exist for this nickel-based CO_2 electroreduction system. Unsupported Ni_3Ga (whose stoichiometry is maintained throughout the bulk and surface) is modestly capable of reducing CO and relatively inactive toward CO_2, but synthesizing films of the alloy on HOPG and vitreous carbon results in an electrochemical reactivity profile that differs from that of the bulk material. Under the conditions described, Ni_3Ga nanoparticles seem largely inactive toward CO_2 reduction. Thin films of Ni_3Ga on different carbon solid supports exhibit dissimilar surface morphologies and reaction mechanisms during CO_2 electroreduction, utilizing a pathway that is either CO-inclusive or CO-exclusive. It appears that the role of a carbon solid support in dictating CO_2 reduction products generated by Ni_3Ga is indirect, as the support exerts control over the catalyst morphology during synthesis. Catalyst morphology then impacts the electrochemical CO_2 reduction reaction that occurs at the material's surface. A summary of electrolysis products obtained using each of the five Ni_3Ga morphologies studied here is presented in Table II.

By exploiting the Ni_3Ga reaction scope and solid support/morphology effect established herein, we were able to make a single catalytic material perform two complementary tasks, ultimately improving upon its ability to generate MeOH from a CO_2 starting material. The importance of solid support choice in achieving particular reaction chemistry has been reported for a handful of systems in the past[25,46–49] and, combined with the data presented here, such results suggest that the structure of a catalyst and the identity of its solid support, when applicable, should be carefully considered in tandem when designing new, or modifying old, heterogenous electrocatalysts. More specifically, carbon solid supports can dictate surface morphology when involved in the material's synthesis, an effect which may be further realized during surface-based catalysis processes such as CO_2 electroreduction.

Acknowledgments

Financial support for this work was provided by the National Science Foundation under grant CHE-1308652. ARP and JJF acknowledge support from the National Science Foundation Graduate Research Fellowship Program under grant Nos. DGE-1148900 and DGE-1656466, respectively. COB thanks the Leach Summer Scholars Program for funding. Any opinions, findings, and conclusions or recommendations expressed in this material are those of the authors and do not necessarily reflect the views of the National Science Foundation.

ORCID

Andrew B. Bocarsly https://orcid.org/0000-0003-3718-0933

References

1. E. Dlugokencky and P. Tans, *Trends in Atmospheric Carbon Dioxide*, NOAA/Earth System Research Laboratory, (2016).
2. *Climate Change Impacts in the United States: The Third National Climate Assessment*, U.S. Global Change Research Program, p. 69 (2014).
3. N. Hoshi, M. Kato, and Y. Hori, *J. Electroanal. Chem.*, **440**, 283 (1997).
4. L. Q. Zhou, C. Ling, M. Jones, and H. Jia, *Chem Commun*, **51**, 17704 (2015).
5. T. Hatsukade, K. P. Kuhl, E. R. Cave, D. N. Abram, and T. F. Jaramillo, *Phys Chem Chem Phys*, **16**, 13814 (2014).
6. C. Kim et al., *J. Am. Chem. Soc.*, **137**, 13844 (2015).
7. A. Salehi-Khojin et al., *J. Phys. Chem. C*, **117**, 1627 (2013).
8. S. Ishimaru, R. Shiratsuchi, and G. Nogami, *J. Electrochem. Soc.*, **147**, 1864 (2000).
9. W. Luc et al., *J. Am. Chem. Soc.*, **139**, 1885 (2017).
10. T. Hatsukade et al., *Energy Technol.*, **5**, 955 (2017).
11. X. Feng, K. Jiang, S. Fan, and M. W. Kanan, *J. Am. Chem. Soc.*, **137**, 4606 (2015).
12. R. B. Rakhi, W. Chen, D. Cha, and H. N. Alshareef, *Nano Lett.*, **12**, 2559 (2012).
13. D. A. Winesett, H. Ade, J. Sokolov, M. Rafailovich, and S. Zhu, *Polym. Int.*, **49**, 458 (2000).
14. Y. Yu et al., *Nano Lett.*, **14**, 553 (2014).
15. L. A. Tietz et al., *J Mater Res*, **4** (1989).
16. M. Hanawa et al., *Jpn. J. Appl. Phys.*, **50**, 053101 (2011).
17. R. Saha and W. D. Nix, *Acta Mater.*, **50**, 23 (2002).
18. J. Zhang et al., *J. Phys. Chem. B*, **108**, 10955 (2004).
19. S. Sun, F. Jaouen, and J.-P. Dodelet, *Adv. Mater.*, **20**, 3900 (2008).
20. L. Xiao, L. Zhuang, Y. Liu, and J. Lu, *J. Am. Chem. Soc.*, **131**, 602 (2009).
21. S. Guo and S. Sun, *J. Am. Chem. Soc.*, **134**, 2492 (2012).
22. Q. Kang et al., *Angew. Chem. Int. Ed.*, **54**, 841 (2015).
23. N. Yang, S. R. Waldvogel, and X. Jiang, *ACS Appl. Mater. Interfaces*, **8**, 28357 (2016).
24. C. M. Elliott and R. W. Murray, *Anal. Chem.*, **48**, 1247 (1976).
25. O. Baturina et al., *Catal. Today*, **288**, 2 (2017).
26. D. A. Torelli et al., *ACS Catal.*, **6**, 2100 (2016).
27. A. R. Paris and A. B. Bocarsly, *ACS Catal.*, 6815 (2017).
28. A. Kirkeminde, S. Spurlin, L. Draxler-Sixta, J. Cooper, and S. Ren, *Angew. Chem.*, **127**, 4277 (2015).
29. A. Kirkeminde and S. Ren, *Chem Commun*, **51**, 8603 (2015).
30. J. L. White and A. B. Bocarsly, *J. Electrochem. Soc.*, **163**, H410 (2016).
31. J. E. Pander, A. Fogg, and A. B. Bocarsly, *ChemCatChem*, **8**, 3536 (2016).
32. Y. Hori, A. Murata, and R. Takahashi, *J. Chem. Soc. Faraday Trans. 1 Phys. Chem. Condens. Phases*, **85**, 2309 (1989).
33. H. Xiao, T. Cheng, W. A. Goddard, and R. Sundararaman, *J. Am. Chem. Soc.*, **138**, 483 (2016).
34. A. G. Pandolfo and A. F. Hollenkamp, *J. Power Sources*, **157**, 11 (2006).
35. P. J. F. Harris, *Philos. Mag.*, **84**, 3159 (2004).
36. A. V. Baranov, A. N. Bekhterev, Y. S. Bobovich, and V. I. Petrov, *Opt. Spektrosk.*, **62**, 612 (1987).
37. Y. Wang, D. C. Alsmeyer, and R. L. McCreery, *Chem. Mater.*, **2**, 557 (1990).
38. J. Wang, *Electrochimica Acta*, **26**, 1721 (1981).
39. J. M. Friedrich, C. Ponce-de-León, G. W. Reade, and F. C. Walsh, *J. Electroanal. Chem.*, **561**, 203 (2004).
40. Y.-J. Zhang, V. Sethuraman, R. Michalsky, and A. A. Peterson, *ACS Catal.*, **4**, 3742 (2014).
41. F. Studt et al., *Nat. Chem.*, **6**, 320 (2014).
42. Z. W. Ulissi et al., *ACS Catal.*, 6600 (2017).
43. I.-F. Hu and Ohio State University thesis, (1985).
44. P. Chen, M. A. Fryling, and R. L. McCreery, *Anal. Chem.*, **67**, 3115 (1995).
45. P. Chen and R. L. McCreery, *Anal. Chem.*, **68**, 3958 (1996).
46. G. Centi, S. Perathoner, G. Win, and M. Gangeri, *Green Chem.*, **9**, 671 (2007).
47. N. R. de Tacconi et al., *Electrochem. Solid-State Lett.*, **15**, B5 (2012).
48. S. Safdar Hossain, S. ur Rahman, and S. Ahmed, *J. Nanomater.*, **2014**, 1–10 (2014).
49. F. Zhou, H. Li, M. Fournier, and D. R. MacFarlane, *ChemSusChem*, **10**, 1509 (2017).